ChemCatChem
The European Society Journal for Catalysis

Chemistry Europe
European Chemical Societies Publishing

Supported by GECATS GERMAN CATALYSIS SOCIETY

Accepted Article

Title: Affecting the Formation of the Micro-structure and Meso/macro-structure of SAPO-34 zeolite by Amphipathic Molecules

Authors: Xuefeng Shen, Yujue Du, Jiajia Ding, Chuanming Wang, Hongxing Liu, Weimin Yang, and Zaiku Xie

To be cited as: *ChemCatChem* 10.1002/cctc.202000794

Link to VoR: https://doi.org/10.1002/cctc.202000794

WILEY-VCH

Affecting the Formation of the Micro-structure and Meso/macro-structure of SAPO-34 zeolite by Amphipathic Molecules

Xuefeng Shen,[b] Yujue Du,[b] Jiajia Ding,[b] Chuanming Wang,[b] Hongxing Liu,*[b] Weimin Yang,*[b] and Zaiku Xie*[a]

[a] Prof. Z. Xie
China Petrochemical Corporation (SINOPEC Group)
Beijing 100728, (P.R. China)
E-mail: xzk@sinopec.com
[b] Dr. X. Shen, Y. Du, J. Ding, Prof. C. Wang, H. Liu, W. Yang
State Key Laboratory of Green Chemical Engineering and Industrial Catalysis
SINOPEC Shanghai Research Institute of Petrochemical Technology,
Shanghai 201208, (P.R. China)
E-mail: liuhx.sshy@sinopec.com，yangwm.sshy@sinopec.com

Supporting information for this article is given via a link at the end of the document.

Abstract: SAPO-34 is an important member in the family of zeolites, which shows excellent catalytic activity in MTO reaction, but suffers from the diffusion bottleneck. To overcome the diffusion problem, porogen was added to generate meso/macro pores in SAPO-34 zeolite. In this work, amphipathic molecules were designed as CSDA to synthesize a tri-level hierarchically porous SAPO-34, and the introduction of CSDA could promote the Si atoms incorporating into the $AlPO_4$ framework, change the morphology of particles and decrease the acidity of prepared SAPO-34 zeolite. The prepared SAPO-34 catalyst exhibits higher selectivity of C_2H_4 and C_3H_6 in the MTO reaction than the conventional SAPO-34 zeolite. The morphology and the microstructure of the prepared samples vary with the carbon chain of the amphipathic molecules due to the matching between amphipathic molecules and topological structure of CHA.

Introduction

Zeolites are crystals with high surface area, adjustable pore size, acidity, high stability and compositional diversity, which are widely used in petrochemical and fine-chemical industries.[1] SAPO-34 is an important member of zeolite, with the topological structure of CHA. SAPO-34 has been considered as an excellent catalyst for the methanol-to-olefin (MTO) conversion, which produces light olefins from nonpetroleum sources, then solves the problem of oil crisis to a great extent.[2] The CHA topological structure of SAPO-34 defines the channel structure of it (cage: 9.4 Å in diameter and 8-ring pore: 3.8 Å × 3.8 Å).[3] The narrow pore opening (~0.38 nm) impedes the diffusion of reactants and leads to rapid deactivation of catalyst.[4] Inspired by the meso-porous materials, introducing meso/macro-pores into SAPO-34 crystals is considered as an efficient way to overcome the inherent diffusion limitations and retard coke deposition to prolong the catalytic lifetime.

Until now, many strategies have been proposed to synthesize hierarchical SAPO-34 zeolite, such as dry gel conversion method,[5] post-treat method,[6] hard template[7] and soft template[8]. Comparing with other strategies, the relatively simple synthetic process, well controlled mesopores and no destruction of Brønsted acid sites of SAPO-34 zeolite make soft template method perferably selected. As for the template method, polymer, cationic surfactant are usually acted as mesoporous template, which only affect the meso/macro-structure of SAPO-34. Yu and coworkers prepared SAPO-34 with the tri-level hierarchically intracrystalline micro-meso-macro-pore structure using PEG 2000 as soft template.[8b] Then, Yu selected [3-(trimethoxysilyl) propyl] octade-cyldimethylammonium chloride (TPOAC) as the meso-pore-generating agent to prepare cubic-shaped micrometer-sized SAPO-34 resulting from the agglomeration of cubic-like nanocrystals,[3b] in which TPOAC acted as not only the soft template, but also a part of the silicon source. Liu and coworkers synthesized hierarchical SAPO-34 with [2-(diethoxyphosphono) propyl]-hexadecyldimethylammonium bromide (DPHAB) as soft template and a part of the phosphor source.[8d]

Quaternary ammoniums are widely used as template to synthesize zeolites. Because the special molecular dimension and steric configuration of quaternary ammoniums make them closely bound to inorganic species, then guided the synthesis of kinds of zeolites.[9] Amphipathic molecules with quaternary ammoniums at both ends are usually used as templates to synthesize hierarchical MFI zeolites.[10] It is notable that only the meso/macro-structure change by tuning the chain length of the intermediate of amphipathic molecules in most cases. Okubo synthesized the hierarchically and sequentially intergrown MFI zeolites by dimers of the tetrapropylammonium cation,[10a] and they found that the lengths of alkyl spacers between two tetrapropylammonium cations affected the morphology of the obtained MFI crystals.[10b] Che used dimers of the N-methyl pyrrolidiniums as templates to synthesize MFI or MTW zeolites via changing the carbon chain lengths,[10d] in which the species of quaternary ammonium is a crucial factor. For different kinds of zeolites, specific amines/ammoniums cooperating with different chain lengths could affect the micro/meso/macro-structure of obtained zeolites, due to dimers of amines/ammoniums with different chain lengths may geometrically matching different zeolite topologies.

Herein, amphipathic molecules were synthesized as the co-structure-directing agent (CSDA), which are dimers of the tetraethylammonium cation connected by carbon chain ($[N^+(CH_2CH_3)_3$-C_nH_{2n}-$N^+(CH_2CH_3)_3]$ $[Br^-]_2$, n = 4, 6, 8, 10, 12, denoted as Cn, Figure S1), because the tetraethylammonium cation is a very common and energetically favored structure-directing agent (SDA) for CHA zeolite formation. In the synthesis of SAPO-34, triethylamine (TEA) was not only as the SDA, but also the alkali source, so TEA still was the SDA in the present work. The prepared SAPO zeolites were well characterized, which showed different morphologies and micro-structures depending on the different carbon chain lengths of CSDA. The status of the CSDA was investigated by various characterizations. The MTO catalytic performance of synthesized SAPO-34 is also evaluated.

Results and Discussion

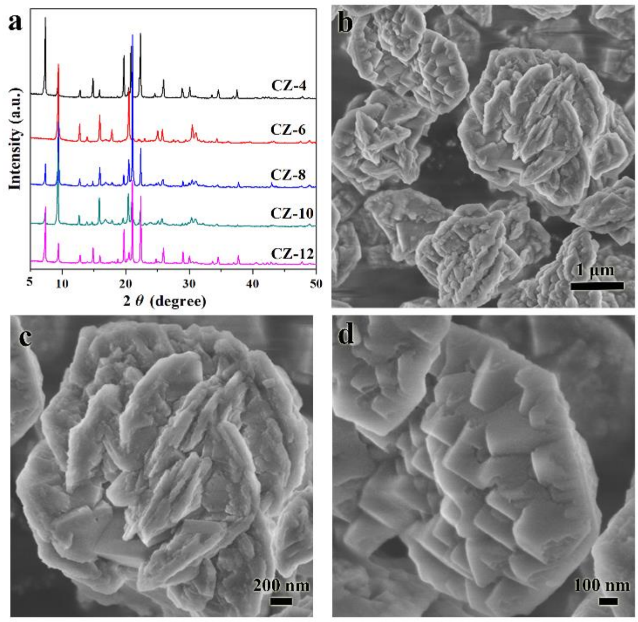

Figure 1. Powder XRD patterns (a) of CZ-4 ~ CZ-12 and SEM images (b-d) of CZ-6.

Well-resolved peaks in the range of 5-50°are observed in the XRD patterns for these SAPO zeolite samples, as shown in Figure 1; The diffraction peaks at 2θ of 9.4, 12.9, 16.1, 20.5, 26.0 and 30.5° are indexed to (101), (110), (021), (12$\bar{1}$), (220) and (401) planes of SAPO-34, respectively;[11] whereas those at 7.5, 14.9, 19.7, 21.1, 22.4 and 26.0° are attributed to (100), (200), (210), (002) and (220) planes of SAPO-5, respectively.[12] Obviously, CZ-6 displays the diffraction peaks of pure phase SAPO-34 with good crystallinity, whereas the CZ-4, CZ-8, CZ-10 and CZ-12 are mixture of SAPO-34 and SAPO-5 zeolites.

The SEM images reveal that CZ-6 exhibits flower-like morphology composed of nanosheets (Figure 1b and 1c), which is very different with the rhombohedral morphology of conventional SAPO-34 (Figure S2). The nanosheet is hexagonal-like with the thickness of ~300 nm and size of ~1 μm. The outside edge of the nanosheet is smooth and the center part is composed of triangular-pyramid-shaped subunits (Figure 1b and 1d). SEM images of other four samples are shown in Supporting Information Figure S3, which also give the evidence that these four samples are mixture of SAPO-34 and SAPO-5 zeolites. The particle size of SAPO-5/SAPO-34 shows no relationship with the carbon chain length of CSDA.

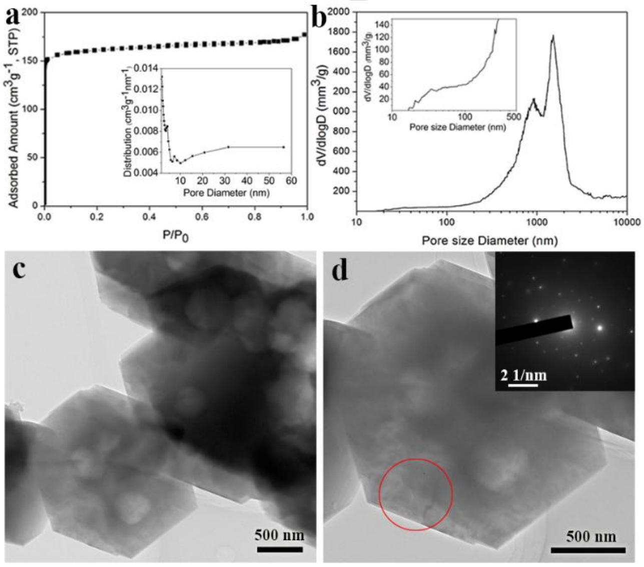

Figure 2. (a) N_2 adsorption and desorption isotherm and pore size distribution curve of CZ-6 (obtained from adsorption branch， inset), (b) pore size distribution curve of CZ-6 determined by mercury intrusion porosimetry. (c-d) TEM images of CZ-6. The selected area diffraction pattern (inset) was taken from the area of the red circle in (d), taken along to the [010] direction of CHA structure.

The N_2 adsorption and desorption isotherm (Figure 2a) of CZ-6 molecule shows the Brunauer-Emmett-Teller (BET) surface area, micropore volume and mesopore volume of this sample are 564 m^2/g, 0.25 cm^3/g and 0.03 cm^3/g, respectively. The pore size distribution curve shows the existence of mesopores in the hierarchically porous CZ-6. The N_2 adsorption and desorption isotherm of other samples are shown in Figure S4, and the textual properties of all samples are shown in Table S1. There is no peaks in the pore size distribution curves of CZ-4, CZ-8, CZ-10 and CZ-12, indicating no mesostructure existence in these samples. Compared with the conventional SAPO-34, the uptakes near saturation pressure in the isotherms of other samples (CZ-4, CZ-6, CZ-8, CZ-10 and CZ-12) are observed, indicating the existence of macropores in these samples. The macropore size distribution determined by mercury intrusion porosimetry shows three different sizes of macropores existing in CZ-6, that is, micrometer-sized macropores (ca. 0.9 μm and 1.5 μm) corresponding to the stacking of the nanosheets and nanometer-sized macrochannels (ca. <100 nm) corresponding to the intracrystalline macropores. The TEM images of CZ-6 show that macropores are existing in the nanosheet, which has a hexagonal-like morphology (Figure 2c-2d). So the CZ-6 is tri-level hierarchical SAPO-34 zeolite with intracrystalline micro-meso-macroporosity.

In order to better understand the effect of carbon chain length of amphipathic molecules for the directing of zeolite framework structures, ab initio molecular dynamics (AIMD) simulations and static structure optimization were employed to evaluate the interaction energies between selected CSDAs and AlPO-34 or AlPO-5 frameworks. The interaction energies of the CSDAs with AlPO-34 and AlPO-5 were depicted in Figure 3, and the optimized structures were shown in Figure 4 and Figure S5. It can be seen that the interaction energy of CSDAs with AlPO-5 decreases linearly with the carbon chain length, indicating that the steric confinement effect is negligible and the van der Waals (vdW) effect dominates the interaction in AlPO-5. In the case of CSDAs in AlPO-34, the interaction between C6-CSDA and AlPO-34 is stronger than that between C4-CSDA/C8-CSDA with AlPO-34 as described by the average interaction energies, agreeing well with the experimental findings. The breaking of linear scaling relations with the carbon chain length indicates that the steric confinement effect is very important for the structure directing effect in AlPO-34. In addition, the interaction energies change obviously with the different configuration of CSDAs in AlPO-34 as indicated by the wide variation range of energy for each CSDA. This is especially obvious for C12-CSDA in AlPO-34. As the interaction energy gradually decreases in AlPO-5 while the steric confinement effect increases with the chain length of CSDAs in AlPO-34, the AlPO-5 structure could not be excluded in the preparation using CSDAs with higher chains. As mentioned above, C6-CSDA could match well with AlPO-34, while C4, C8, C10 and C12 molecules are more favorable fitting in the channel of AlPO-5 as a result of vdW stabilization interaction and steric repulsion interaction.

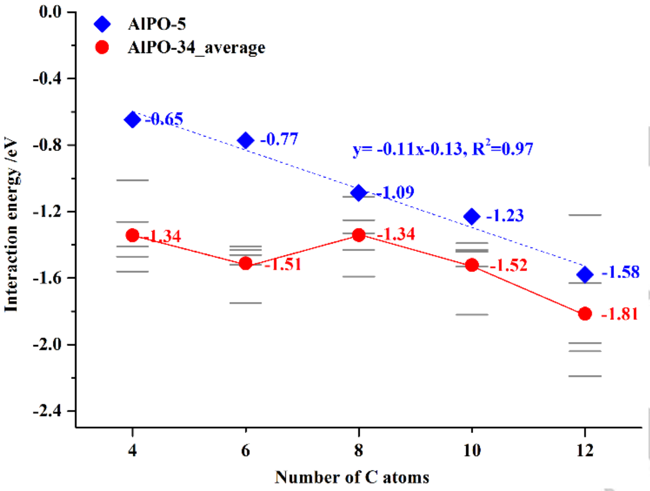

Figure 3. Interaction energies of CSDAs with different carbon chain lengths in AlPO-34 and AlPO-5 frameworks. The energies of five different configurations of each CSDA in AlPO-34 were depicted in grey line and the average value were depicted in red.

According to the theoretical calculations, C6 molecules locate in the adjacent cages of CHA structure during the synthesis process of CZ-6, as shown in Figure 4. The tetraethylammonium cation is also widely used in synthesizing SAPO-34 zeolite. So C6 molecules could cooperate with TEA molecules to direct the formation of the crystalline frameworks of CHA, resulting in pure phase SAPO-34 with flower-like morphology. At the early stage of synthesis, a particular crystal morphology composed of pyramidal parts were generated, due to the growth of CHA preferentially along certain directions.[13] For the conventional SAPO-34 zeolite, pyramidal parts grow to form a regular-shaped rhombohedral crystal with further ageing.[13a] In the synthesis procedure of CZ-6, C6 molecules may act as the crystal growth inhibitor in the next stage, preventing the growth of pyramidal parts to rhombohedral crystal. Meanwhile, C6 molecules may also act as the porogen to generate meso/macro-pores in the SAPO-34 crystals, due to the strong interaction of tetraethylammonium cations and aluminophosphate precursor species. Flower-like SAPO-34 with tri-level hierarchical structure was generated with the combination of TEA and C6. For C4, C8, C10 and C12 molecules, they could not load in the cages of CHA mainly due to the steric repulsion interaction, and they tended to load in the channel of SAPO-5, leading to the formation of SAPO-5 crystals. With further ageing, they may also act as crystal growth inhibitor to decrease the size of SAPO-5 crystals (C4, Figure S3a) or porogen to generate macro-pores in SAPO-5 crystals (C8, C10 and C12, Figure S3b-S3d, Table S1).

The chemical environment of the framework atoms in CZ-6 and conventional SAPO-34 was evaluated by ^{27}Al, ^{31}P, and ^{29}Si MAS NMR. The ^{27}Al MAS NMR spectrum (Figure 5a) proved the presence of tetrahedrally coordinated Al (signal at ca. 35 ppm) and octahedrally coordinated framework Al (signal at ca. -10 ppm).[14] The signals at -3.2 ppm and 75 ppm might be attributed to the formation of $[Al(H_2O)_5(PO\text{-})]^{2+}$ species and Al(OSi)x species.[15] The dominating signals at -30 ppm in the ^{31}P MAS NMR spectra (Figure 5b) is assigned to tetrahedrally coordinated phosphorus atoms in the coordination state of $(P(OAl)_4)$.[13a, 16] The signals at -6 ppm and -55 ppm are from spinning sidebands.[17] In the ^{29}Si MAS NMR spectra (Figure 5c), the signals with a chemical shift of about -91 ppm is assigned to the coordination state of Si(0Si4Al), and the peaks around -94 ppm, -100 ppm and -105 ppm are ascribed to the Si(1Si3Al), Si(2Si2Al) and Si(3Si1Al), respectively.[13a,18] The signal at about -110 ppm is ascribed to the Si(4Si0Al), demonstrating the existence of Si islands, which is very weak compared with these dominate signals. The CZ-6 crystal shows more tetrahedrally aluminum atoms as well as less coordination state of $(P(OAl)_4)$ than conventional SAPO-34 crystal, and the results of XRF (X-ray Fluorescence)

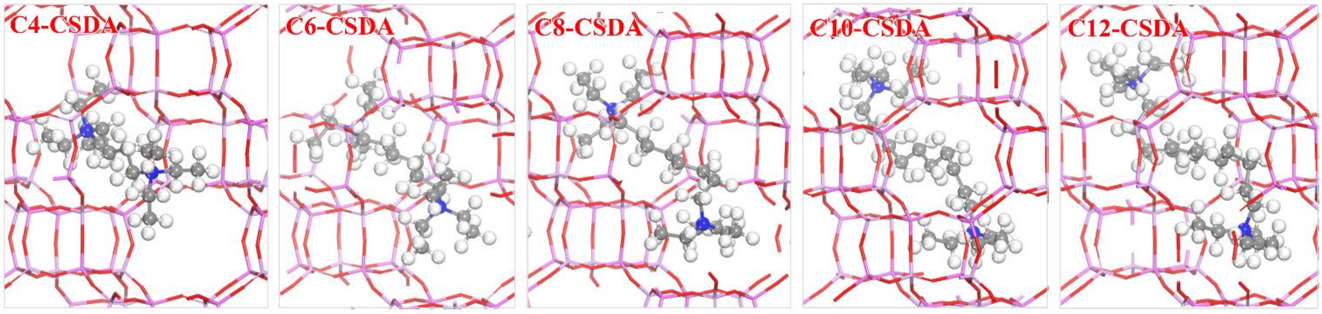

Figure 4. Optimized representative structures of CSDAs with different carbon chain lengths in AlPO-34.

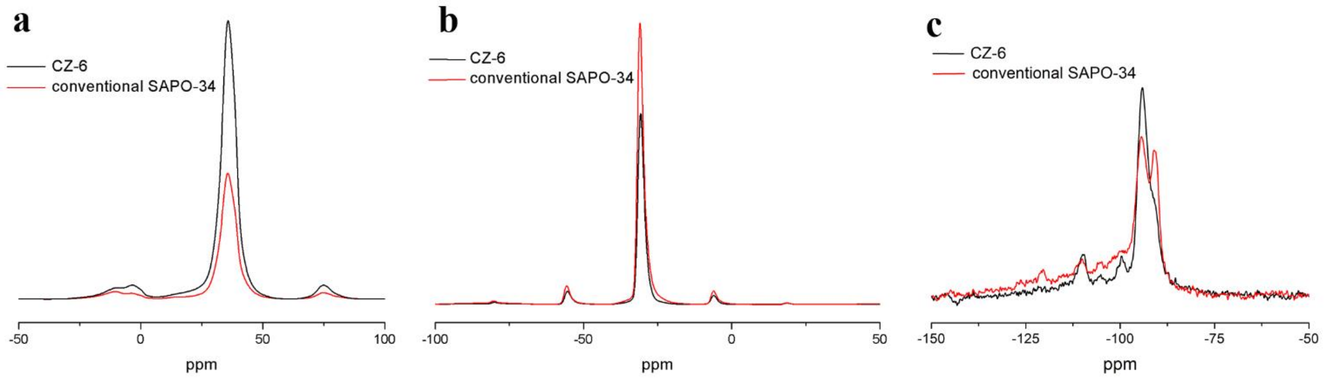

Figure 5. ^{27}Al (a), ^{31}P (b) and ^{29}Si (c) MAS NMR spectra of calcined CZ-6 and calcined conventional SAPO-34.

show the CZ-6 has higher silica content and lower phosphorus content than the conventional SAPO-34 (Table 1), which indicates that C6 molecules promotes the incorporating of Si atoms into the $AlPO_4$ framework mainly by SM2 mechanism and less partly by SM3 mechanism. The CZ-6 crystal shows coordination state of Si(1Si3Al), Si(2Si2Al) and Si(4Si0Al) increase, especially for Si(1Si3Al), indicating the size of Si islands is small.[19] The coordination state of Si(0Si4Al) decrease, which is the main source of the bridge hydroxyl groups of Si(OH)Al.[17] Due to the Brønsted acid originates from the bridging hydroxyl groups,[19] the CZ-6 shows lower Brønsted acid concentration.

Table 1. The XRF results of CZ-6 and conventional SAPO-34 (mol %).

Samples	Al_2O_3	SiO_2	P_2O_5
CZ-6	46.58	8.43	44.99
Conventional SAPO-34	46.89	6.69	46.41

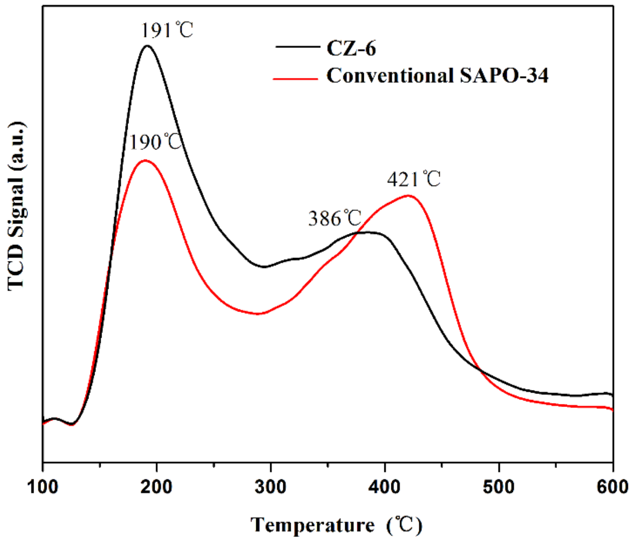

Figure 6. The NH_3-TPD curves of CZ-6 and the conventional SAPO-34.

Figure 6 shows the NH_3-TPD profiles of the CZ-6 and the conventional SAPO-34, which is used to evaluate the acidity of samples. The strength and concentration of acid sites are represented by desorption temperature and the peak area, respectively. The conventional SAPO-34 shows two desorption peaks centered at about 190℃ and 421℃, which correspond to the weak and strong acid sites, respectively.[5] For CZ-6, the desorption temperature of the weak acid site is nearly the same with the conventional SAPO-34, while the desorption temperature of the strong acid site is obviously lower than the conventional SAPO-34. The weak acid site is attributed to T-OH (T = Si, P, Al) hydroxyl groups or lattice imperfection;[8a, 16, 20] and the strong acid site is mainly attributed to the adsorption of NH_3 on the Brønsted acid sites,[21] which have close relationship with the MTO catalytic properties.[22] The strength of the Brønsted acid of CZ-6 is obviously weaker than that of the conventional SAPO-34.

The solid ^{13}C NMR spectra of as-made conventional SAPO-34, as-made CZ-6 and C6 (Figure S6) are used to verify C6 molecules keeping intact during the entire synthetic process. The thermogravimetric analyses (TGA) curve (Figure S7) of CZ-6 shows that the content of template molecules in the as-made CZ-6 is approximately 19.6 wt %, larger than that of conventional SAPO-34 (18.2 wt %), due to the additional C6 molecules in CZ-6. Two obvious weight losses can be recognized from TGA curves: a low-temperature weight loss before 150°C and a high-temperature weight loss after 300°C, which are ascribed to desorption of water and templates, respectively.[23] The template molecule begins to decompose after 300°C, which is obviously higher than the crystallization temperature, so the TGA curve also give the evidence that C6 molecules keep intact during the entire synthetic process.

Catalytic tests of methanol conversion were performed in a fixed bed reactor at 733 K over the CZ-6 and conventional SAPO-34 catalysts. The selectivity of C_2H_4 and C_3H_6 *versus* TOS over CZ-6 and conventional SAPO-34 catalysts are shown in Figure 7a, and the detailed MTO results are summarized in Table S2. Compared with the conventional SAPO-34, CZ-6 shows higher selectivity of C_2H_4 and C_3H_6, and the difference in selectivity increases with the TOS. The selectivity of C_2H_4 and C_3H_6 of CZ-6 (85.05%) has improved nearly 3% compared to that of the conventional SAPO-34 (81.99%), which is mainly due to the lower acidity concentration and relatively weaker acid strength of CZ-6.[22] Hydrogen transfer is the major route in catalytic conversion of MTO for the formation of nonolefinic byproducts,[24] which mainly take place on Brønsted acid sites (Si-OH-Al).[25] The CZ-6 shows lower acidity than the conventional SAPO-34, which make it less reactive for the hydrogen transfer compared with the conventional SAPO-34, leading to a higher selectivity to light olefins.[26] The hierarchical porosity is also beneficial to improve

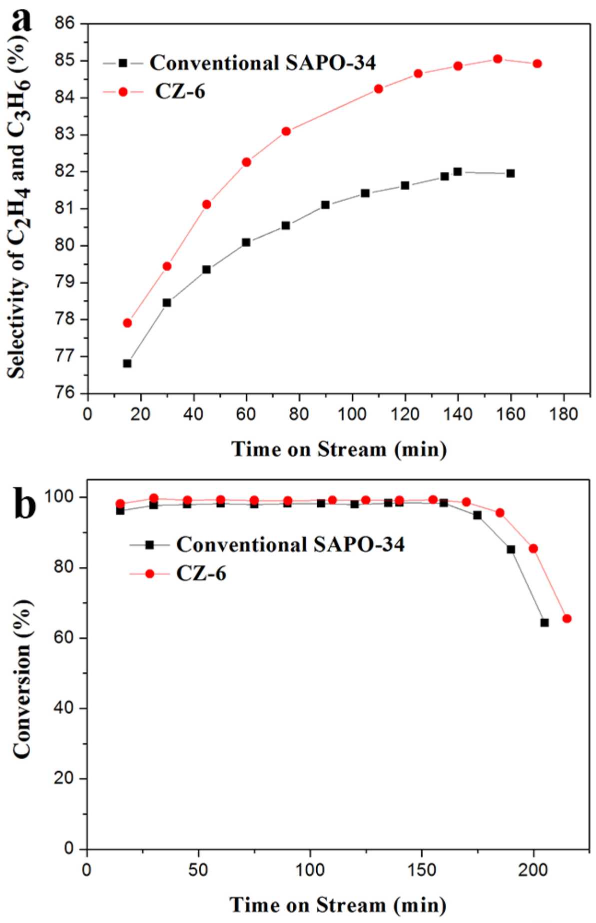

Figure 7. Catalytic performance of CZ-6 and conventional SAPO-34 in the MTO reaction: (a) the selectivity of C_2H_4 and C_3H_6 variation with time-on-stream (TOS) and (b) methanol conversion variation with TOS. Experimental conditions: WHSV = 2.4 h^{-1}, T = 733 K, catalyst weight = 2 g, 40% methanol.

the catalytic activity and selectivity.[3b, 27] Besides, the lifetime of CZ-6 is longer than the conventional SAPO-34 (Figure 7b). The tri-level structure of CZ-6 can greatly enhance the diffusion efficiency of products from narrow pores to outside space, then reduces the coke formation, which effectively prolong the lifetime and improve the product selectivity.[8b, 27] Meanwhile, the decreased acidic strength and acidic concentration of CZ-6 catalysts can also retard the coke formation and thus prolong the lifetime of CZ-6.[28]

Conclusion

In summary, the amphipathic molecules, consisting of dimers of the tetraethylammonium cation connected by carbon chain, affect the formation of micro-structure and meso/macro-structure of SAPO-34 zeolite. Only C6 molecules can cooperate with TEA to directly synthesize the tri-level hierarchically porous SAPO-34 zeolite, which has flower like morphology. The C6 molecules not only serve as the porogen to generate hierarchical structure, but also inhibit the growth of pyramidal parts, formed in the early stage, growing to rhombohedral crystal. It also can be found that the introduction of C6 molecules promotes Si atoms into the $AlPO_4$ framework, and decrease the acidity of the prepared SAPO-34 zeolite. The CZ-6 exhibits superior MTO performance with the selectivity of C_2H_4 and C_3H_6 up to 85.01%, which has improved more than 3% than the conventional SAPO-34. For C4, C8, C10 or C12, the products are mixture of SAPO-34/5, as a result of the mismatch between CSDA with the CHA structure of SAPO-34. This work demonstrates that adding amphipathic molecules is an effective way to control meso/macro structure and affect the formation of micro-structure of SAPO-34 zeolite. We hope our strategy will provide a new way for the design and synthesis of hierarchical SAPO-34 for high catalytic activity.

Experimental Section

Materials

Orthophosphoric acid (H_3PO_4, 85 wt%), TEA (99 wt%), acetonitrile (99 wt%), diethyl ether (99 wt%), colloidal silica (SiO_2, 40 wt%), pseudoboehmite (Al_2O_3, 70 wt%), 1,4-dibromobutane (98 wt%), 1,6-dibromohexane (98 wt%), 1,8-dibromooctanewere (98 wt%), 1,10-dibromodecane (98 wt%) and 1,12-dibromododecane (98 wt%) were purchased from Sinopharm Chemical ReagentCo., Ltd. All chemicals were used as received without further purification.

Synthesis of Cn

10.8 g of 1,4-dibromobutane (0.05 mol) and 10.25 g (0.25 mol) of triethylamine were mixed in 150 ml of acetonitrile and stirred at 84 ℃ for 12 h. Then removal of acetonitrile by rotary evaporator and the $[N^+(CH_2CH_3)_3\text{-}C_nH2_n\text{-}N^+(CH_2CH_3)_3]\ [Br^-]_2$, (C4) was filtered and washed with diethyl ether three times. Then C4 was dried in a vacuum. C6, C8, C10 and C12 were also obtained by substituting 4-dibromobutane with 1, 6-dibromohexane, 1, 8-dibromooctane, 1,10-dibromodecane and 1,12-dibromododecane. The molecule structure are shown in supporting information (Figure S1).

Synthesis of SAPO-34/ SAPO-5

A typical synthesis procedure was as follows. A certain amount of pseudoboehmite was firstly added into deionized water. Then, desired amount of phosphoric acid was added in sequence. After further stirring for 3 h, a certain amount of triethylamine was added in the obtained gel and stirred for 1h. Then colloidal silica and Cn were added in sequence and stirred for 12h. Then the obtained gel was transferred into a stainless steel autoclave and heated rotationally (15 rpm) at 200 ℃ for 24h and 120 ℃ for 10h under autogenous pressure. The products were recovered by filtration, washed with deionized water and dried in air. The molar composition of the gel is 0.5Cn : $1.0P_2O_5$: $1.0Al_2O_3$: $0.38SiO_2$: 3.0TEA : $59H_2O$. The product donated as CZ-n (n = 4, 6, 8, 10, 12). For comparison, conventional SAPO-34 was prepared by using the corresponding SDA but without any CSDA.

Computational details

The AlPO-34 framework was represented by a periodic 36T hexagonal cell, and the AlPO-5 framework was represented by 96T super cell constructed by repeating the unit cell forth in direction of the twelve-membered channel. All density functional theory (DFT) calculations were performed using VASP software with Grimme-D3 corrected Perdew-Burke-Ernzerhof XC functional (PBE-D3). The projector augmented wave (PAW) was used to describe electronic interaction with the plane wave basis set kinetic energy cutoff equal to 400 eV. The sampling of Brillouin zone was only with Γ point. A force threshold of 0.02 eV/Å was employed for structure optimization. The AIMD simulations were performed using NVT ensemble at 873 K for 10 ps with a time step of 1 fs to relax the structure of SDAs in AlPO-34. Five structures were selected every 2 ps for structure optimization. The positive charge of CSDAs was balanced by the background charge of the system, and the energetics were calibrated using charged ammonia for the comparison of interaction energies of CSDAs in AlPO-34 and AlPO-5.

Characterization

XRD patterns were obtained using Bruker D8 Advance diffractometer, with an accelerated voltage of 40 kV and detector current of 200 mA. Cu-Kα radiation (λ = 51.540589 Å) was used for a continuous scanning with the step-size of 0.02° over a 2θ range of 5-50°. X-ray fluorescence spectroscopy was obtained on Bruker S4 Pioneer. N_2 Adsorption and desorption isotherms were collected on Micromeritics TriStar3000 at 75 K. Prior to the measurements, the sample was degassed at 350 °C until a stable vacuum of about 0.67 Pa was reached. FE-SEM (Field Emission Scanning Electron Microscopy) analysis was performed on a Hitachi S4800 electron microscope with an accelerating voltage of 2.0 kV. HRTEM was performed using JEOL JEM-2100LaB6 operating at 200 kV (Cs = 1.0 mm, point resolution of 2.3 Å). Images were recorded with a Keen View CCD camera (resolution of 1376 pixels × 1032 pixels, pixel size of 6.45 μm × 6.45 μm) at 50000−120000× magnification under low-dose conditions. The ^1H NMR, ^{13}C NMR spectra and solid-state MAS NMR were recorded on an JNM-ECZ500R/S1 spectrometer with chemical shifts reported in ppm relative to the residual deuterated solvent and the internal standard tetramethylsilane (TMS). Temperature-programmed desorption of ammonia (NH_3-TPD) experiments were performed on a chemisorption analyzer (FINETEC FINSORB-3010). Mercury intrusion porosimetry was obtained on Pascal 140/240, produced by Thermo Electron. TGA curves were performed on TGA 7 thermogravimetric analyzer (Perkin Elmer, Inc., USA). The heating rate was 20 °C/min. The results of XRF were obtained on XRF-1800, produced by SHIMADZU.

Catalytic tests

The reaction products were analyzed using an on-line gas chromatograph (Agilent GC 7890N), equipped with a flame ionization detector (FID) and Plot-Q column (Agilent J&W GC Columns, HP-PLOT/Q 19091-Q04, 30 m × 320 μm × 10 μm). The conversion and selectivity were calculated on CH_2 basis and dimethyl ether (DME) was considered as reactant in the calculation.

Acknowledgements

This work was supported by the National Key Research and Development Program of China (Grant No. 2016YFB0701100).

Keywords: Amphipathic molecules • Geometrical matching • Hierarchical zeolite • SAPO-34 zeolite

[1] a) A. Corma, *Chem. Rev.* 1995, 95, 559-614; b) W. F. Hölderich, G. Heitmann, *Catal. Today* 1997, 38, 227-233; c) M. J. Verhoef, P. J. Kooyman, J. C. van der Waal, M. S. Rigutto, J. A. Peters, H. van Bekkum, *Chem. Mater.* 2001, 13, 683-687; d) C. S. Cundy, P. A. Cox, *Chem. Rev.* 2003, 103, 663-702; e) J. Čejka, B. Wichterlová, *Catal. Rev.; Sci. Eng.* 2002, 44, 375-421.

[2] a) U. Olsbye, S. Svelle, M. Bjørgen, P. Beato, T. V. W. Janssens, F. Joensen, S. Bordiga, K. P. Lillerud, *Angew. Chem., Int. Ed.* 2012, 51, 5810-5831; b) P. Tian, Y. X. Wei, M. Ye, Z. M. Liu, *ACS Catal.* 2015, 5, 1922-1938.

[3] a) B. M. Lok, C. A. Messina, R. L. Patton, R. T. Gajek, T. R. Cannan, E. M. Flanigen, *J. Am. Chem. Soc.* 1984, 106, 6092-6093; b) Q. M. Sun, N. Wang, D. Y. Xi, M. Yang, J. H. Yu, *Chem. Commun.* 2014, 50, 6502-6505.

[4] X. C. Zhu, J. P. Hofmann, B. Mezari, N. Kosinov, L. L. Wu, Q. Y. Qian, B. M. Weckhuysen, S. Asahina, J. Ruiz-Martínez, E. J. M. Hensen, *ACS Catal.* 2016, 6, 2163-2177.

[5] H. Q. Yang, Z. C. Liu, H. X. Gao, Z. K. Xie, *J. Mater. Chem.* 2010, 20, 3227-3231.

[6] a) X. X. Chen, A. Vicente, Z. X. Qin, V. Ruaux, J. P. Gilson, V. Valtchev, *Chem. Commun.* 2016, 52, 3512-3515; b) Y. Y. Qiao, M. Yang, B. B. Gao, L. Y. Wang, P. Tian, S. T. Xu, Z. M. Liu, *Chem. Commun.* 2016, 52, 5718-5721.

[7] F. Schmidt, S. Paasch, E. Brunner, S. Kaskel, *Microporous Mesoporous Mater.* 2012, 164, 214-221.

[8] a) Y. Cui, Q. Zhang, J. He, Y. Wang, F. Wei, *Particuology* 2013, 11, 468-474; b) Q. M. Sun, N. Wang, G. Q. Guo, X. X. Chen, J. H. Yu, *J. Mater. Chem. A* 2015, 3, 19783-19789; c) L. T. Kong, B. X. Shen, Z. Jiang, J. G. Zhao, J. C. Liu, *React. Kinet., Mech. Cat.* 2015, 114, 697-710; d) C. Wang, M. Yang, W. N. Zhang, X. Su, S. T. Xu, P. Tian, Z. M. Liu, *RSC Adv.* 2016, 6, 47864-47872.

[9] a) X. H. Bu, P. Y. Feng, G. D. Stucky, *Science* 1997, 278, 2080-2085; b) M. Moliner, F. Rey, A. Corma, *Angew. Chem., Int. Ed.* 2013, 52, 13880-13889; c) S. Ramzy M, *J. Am. Chem. Soc.* 2011, 46, 18728-18741; d) R. Francis, D. O'Hare, *J. Chem. Soc., Dalton Trans.* 1998, 19, 3133-3148; e) B. M. Lok, T. R. Cannan, C. A. Messina, *Zeolites* 1983, 3, 282-291.

[10] a) W. Chaikittisilp, Y. Suzuki, R. R. Mukti, T. Suzuki, K. Sugita, K. Itabashi, A. Shimojima, T. Okubo, *Angew. Chem.* 2013, 125, 3439-3443; b) S. H. Keoh, W. Chaikittisilp, K. Muraoka, R. R. Mukti, A. Shimojima, P. Kumar, M. Tsapatsis, T. Okubo, *Chem. Mater.* 2016, 28, 8997-9007; c) D. D. Xu, Y. H. Ma, Z. F. Jing, L. Han, B. Singh, J. Feng, X. F. Shen, F. L. Cao, P. Oleynikov, H. Sun, O. Terasaki, S. A. Che, *Nat. Commun.* 2014, 5, 4262; d) X. L. Jia, Y. J. Zhang, Z. Gong, B. Wang, Z. G. Zhu, J. G. Jiang, H. Xu, H. Sun, L. Han, P. Wu, S. A. Che, *J. Phys. Chem. C* 2018, 122, 9117-9126; e) D. D. Xu, Z. F. Jing, F. L. Cao, H. Sun, S. A. Che, *Chem. Mater.* 2014, 26, 4612-4619.

[11] S. Aghamohammadi, M. Haghighi, M. Charghand, *Mater. Res. Bull.* 2014, 50, 462-475.

[12] B. B. Gao, P. Tian, M. R. Li, M. Yang, Y. Y. Qiao, L. Y. Wang, S. T. Xu, Z. M. Liu, *J. Mater. Chem. A* 2015, 3, 7741-7749.

[13] a) D. Y. Xi, Q. M. Sun, J. Xu, M. Cho, H. S. Cho, S. Asahina, Y. Li, F. Deng, O. Terasaki, J. H. Yu, *J. Mater. Chem.* A 2014, 2, 17994-18004; b) L. Karwacki, E. Stavitski, M. H. F. Kox, J. Kornatowski, B. M. Weckhuysen, *Angew. Chem., Int. Ed.* 2007, 46, 7228-7231.

[14] a) A. Buchholz, W. Wang, M. Xu, A. Arnold, M. Hunger, *J. Phys. Chem. B* 2004, 108, 3107-3113; b) T. H. Chen, B. H. Wouters, P. J. Grobet, *J. Phys. Chem. B* 1999, 103, 6179-6184.

[15] a) Ø. B. Vistad, E. W. Hansen, D. E. Akporiaye, K. P. Lillerud, *J. Phys. Chem. A* 1999, 103, 2540-2552; b) A. V. McCormick, A. T. Bell, C. J. Radke, *J. Phys. Chem.* 1989, 93, 1741-1744.

[16] Q. M. Sun, Y. H. Ma, N. Wang, X. Li, D. Y. Xi, J. Xu, F. Deng, K. B. Yoon, P. Oleynikov, O. Terasaki, J. H. Yu, *J. Mater. Chem. A* 2014, 2, 17828-17839.

[17] G. J. Yang, Y. X. Wei, S. T. Xu, J. R. Chen, J. Z. Li, Z. M. Liu, J. H. Yu, R. R. Xu, *J. Phys. Chem. C* 2013, 117, 8214-8222.

[18] a) J. Tan, Z. M. Liu, X. H. Bao, X. C. Liu, X. W. Han, C. Q. He, R. S. Zhai, *Microporous Mesoporous Mater.* 2002, 53, 97-108; b) T. Álvaro-Muñoz, C. Márquez-Álvarez, E. Sastre, *Appl. Catal., A* 2014, 472, 72-79.

[19] W. L. Shen, X. Li, Y. X. Wei, P. Tian, F. Deng, X. W. Han, X. H. Bao, *Microporous Mesoporous Mater.* 2012, 158, 19-25.

[20] X. T. Wang, R. Li, S. U. H. Bakhtiar, F. L. Yuan, Z. B. Li, Y. J. Zhu, *Catal. Commun.* 2018, 108, 64-67.

[21] B. B. Gao, M. Yang, Y. Y. Qiao, J. Z. Li, X. Xiang, P. F. Wu, Y. X. Wei, S. T. Xu, P. Tian, Z. M. Liu, *Catal. Sci. Technol.* 2016, 6, 7569-7578.

[22] D. Fan, P. Tian, S. T. Xu, D. H. Wang, Y. Yang, J. Z. Li, Q. Y. Wang, M. Yang, Z. M. Liu, *New J. Chem.* 2016, 40, 4236-4244.

[23] I. Miletto, C. Ivaldi, G. Paul, S. Chapman, L. Marchese, R. Raja, E. Gianotti, *ChemistryOpen* 2018, 7, 297-301.

[24] S. Muller, Y. Liu, F. M. Kirchberger, M. Tonigold, M. Sanchezsanchez, J. A. Lercher, *J. Am. Chem. Soc.* 2016, 138, 15994-16003.

[25] a) S. Ilias, A. Bhan, *ACS Catal.* 2013, 3, 18-31; b) S. Ilias, A. Bhan, *J. Catal.* 2012, 290, 186-192.

[26] a) I. Yarulina, A. D. Chowdhury, F. Meirer, B. M. Weckhuysen, J. Gascon, *Nat. Catal.* 2018, 1, 398-411; b) J. J. Su, H. B. Zhou, S. Liu, C. M. Wang, W. Q. Jiao, Y. D. Wang, C. Liu, Y. C. Ye, L. Zhang, Y. Zhao, H. X. Liu, D. Wang, W. M. Yang, Z. K. Xie, M. Y. He, *Nat. Commun.* 2019, 10, 1297.

[27] B. Li, Z. J. Hu, B. Kong, J. X. Wang, W. Li, Z. K. Sun, X. F. Qian, Y. S. Yang, W. Shen, H. L. Xu, D. Y. Zhao, *Chem. Sci.* 2014, 5, 1565-1573.
[28] M. Kang, T. Inui, *Catal. Lett.* 1998, 53, 171-176.